STATIC TESTING AND ANALYSIS OF THE TALLYSMAN VERAPHASE VP6000 GNSS ANTENNA

Ryan M. White and Richard B. Langley

Geodetic Research Laboratory
Department of Geodesy and Geomatics Engineering
University of New Brunswick
P.O. Box 4400
Fredericton, New Brunswick
Canada
E3B 5A3

February 2018

Introduction

One often overlooked aspect of a GNSS receiver system is the selection of an appropriate GNSS antenna. While many currently-available antennas are capable of delivering reasonable geodetic-quality positioning, navigation, and timing (PNT) solutions, recent advances in GNSS antenna technology are helping to provide products with improved performance for PNT users. One such product is the Tallysman VeraPhase VP6000 GNSS antenna. With improved performance characteristics including very low cross-polarization, very low back radiation, very high phase-center stability, and a compact structure as well as sufficient bandwidth to receive all existing and currently-planned GNSS signals, the VP6000 will allow users to enhance the quality of their PNT solutions.

While the VP6000 antenna has been extensively tested using simulated GNSS data, further testing using GNSS observables collected in real-world environments is required in order to determine the actual performance enhancements associated with its novel design. Recently, kinematic tests of the antenna have been carried out by mounting it to the roof of a vehicle and making GNSS measurements in urban and suburban environments (White and Langley, 2017a). Another area of interest is the performance of the VP6000's static data collection in high-multipath environments. A preliminary test of the VP6000's performance in static data collection was carried out by making GNSS measurements at 1- and 2-meter antenna heights in an enclosed sports dome where overhead steel support structures, concrete and steel flooring, and nearby lighting equipment introduced significant multipath errors (White and Langley, 2017b). As a means of further assessing the antenna's capabilities in a static, high-multipath environment, the Tallysman VP6000 was used to track GNSS observables on the roof of the University of New Brunswick's Gillin Hall where the adjacent building structures and concrete and steel flooring were sure to introduce multipath errors.

Equipment

Equipment utilized in this work included the following:

- Tallysman VeraPhase VP6000 antenna
  - SN: 603500018161005
- AOAD/M_T Choke-Ring antenna
  - SN: 283
- Leica AX1203+ GNSS antenna
  - SN: NEH09: 30029
- Javad Triumph-LS GNSS receivers
  - SN: 1WUDUI793SGLZ611LGYHOEA9DT, 1WUDUDHST4SD39F1LGYHOEA9DT, and 1WUDUFTNXJCCIJ11LGYHOEA9DT

Methodology

In order to provide a comparison of the performance of the Tallysman antenna against other geodetic-quality GNSS antennas on the market, observations were also collected using an AOA choke-ring antenna as well as a Leica AX1203+ GNSS antenna. From approximately 01:00-23:00 UTC on days of year (DOY) 278-280, 283-285, and 287-289 (2017), 9 different static data collection sessions were held. For DOY 278-280, 283-285, and 287-289, the Tallysman VP6000, AOA choke-ring, and Leica

AX1203+ antennas were affixed to tripods setup over 3 different steel pillars at heights of approximately 1, 2, and 1.5 metres, respectively (Figures 1-3), and paired with 3 Javad Triumph LS GNSS receivers (Figure 4). For DOYs 278-280, each antenna was rotated around the three different tripods set at 1-metre antenna heights. This process of rotation was again performed at 2- and 1.5-metre antenna heights for DOYs 283-285 and 287-289, respectively. Initially, it was intended to use a height of 3 metres for the final set of observations (DOYs 287-289), but due to predicted high winds and safety concerns, it was decided to change the height of the final series of observations to 1.5 metres. Each receiver was capable of logging multi-GNSS data from both the Global Positioning System (GPS) and Galileo, including GPS L1/L2/L5 and Galileo E1/E5a/E5/E5b carrier-phase and pseudorange observables. Observations for each of the 9 static data collection sessions were logged to the internal memory of the Javad receivers at a 30-second data interval using a 0° elevation angle cutoff threshold.

Figure 1: Tallysman VeraPhase VP6000 (left), Leica AX1203+ (middle), and AOA choke-ring (right) antennas set on tripods at a 1-metre height on DOY 278-280.

Figure 2: Tallysman VeraPhase VP6000 (left), Leica AX1203+ (middle), and AOA choke-ring (right) antennas set on tripods at 2-metres height on DOY 283-285.

Figure 3: Tallysman VeraPhase VP6000 (left), Leica AX1203+ (middle), and AOA choke-ring (right) antennas set on tripods at a 1.5-metre height on DOY 287-289.

Figure 4: Javad Triumph LS receivers connected to the Tallysman VP6000, AOA choke-ring, and Leica AX1203+ antennas on the roof of Gillin Hall.

Following the data collection, 27 (3 antennas x 3 heights x 3 pillars/day) separate RINEX v3.02 files were generated representative of different observation periods for each antenna type. These RINEX 3.02 files were then post-processed using the University of New Brunswick's GNSS Analysis and Positioning Software (GAPS) precise point positioning (PPP) utility to obtain estimates of receiver position as well as to assess metrics including receiver position, carrier-phase and pseudorange residual behavior, and multipath mitigation. All observations were processed in static mode (assuming a stationary, fixed antenna) by GAPS using a 10° elevation angle cutoff threshold. A maximum geometric dilution of precision (GDOP) threshold of 20 was applied as a means of quality control. Epochs with cycle-slips detected using an algorithm by Blewitt [1990] were flagged and their corresponding ambiguities were reset as a means of additional quality control. Observables used in processing include the GPS L1/L2 pseudorange (C1W/C2W) and carrier-phase (L1W/L2W) as well as the Galileo

E1/E5a/E5b/E5 pseudorange (C1X/C5X/C7X/C8X) and carrier-phase (L1X/L5X/L7X/L8X) observables. These abbreviations for the observables are RINEX 3.xx designators.

While the International GNSS Service (IGS) final orbit and clock products were used for GPS-only processing, the IGS Multi-GNSS Experiment (MGEX) orbits and clocks provided by the University of Bern's Astronomical Institute Center for Orbit Determination in Europe (CODE) were used for all GPS + Galileo processing. The IGS final and IGS MGEX CODE orbit products are available at a 15-minute and 5-minute interval, respectively, while satellite clock correction products from both providers are available at a 30-second interval. The use of CODE products was selected for this work since they provided satellite clock corrections at the same sampling interval as the observations, thus allowing for mitigation of errors attributed to clock interpolation. Previous research has also shown that the CODE orbits and clocks can be used to obtain reasonable accuracies in position estimates as compared to the use of other IGS MGEX products [White and Langley, 2015]. Use of the IGS MGEX products further allows for the mitigation of differences between satellite systems, commonly referred to as inter-system biases (ISBs), including the use of each system's independent geodetic reference frame and system time (e.g. GPS Time and Galileo System Time). To account for residual ISB errors as well as frequency- and system-dependent hardware delays, GAPS estimates combined ISB parameters within its existing sequential least-squares filter for Galileo observables.

Standard IGS ANTEX antenna calibrations were used for the application of antenna-specific (GPS) satellite and receiver phase-centre offsets (Schmid et al., 2005). For all Galileo satellite antenna phase-centre offsets, standard IGS MGEX values of (-170.0, +30.0, +950.0) mm and (+160.0, -10.0, +1050.0) mm were used for the in-orbit-validation (IOV) and full-operational-capability (FOC) satellites, respectively (Montenbruck et al., 2014). For this work, no Galileo receiver antenna phase-centre offsets were applied. To mitigate the effects of neutral atmosphere delay (NAD), the VMF1 (gridded) NAD prediction model (Nievinski, 2009) was applied for the a priori delay and mapped to a slant delay using the Vienna mapping functions (Boehm et al., 2006). Residual NAD was additionally estimated at each epoch as a least-squares parameter and applied to the modeled observables. Tropospheric gradients were not estimated or applied during any of the processing. First-order ionospheric delay was mitigated through use of the iono-free linear combination of observables. Other corrections, including those for ocean and body tide loading, Sagnac and relativistic effects, and phase wind-up were also applied to the modelled observables during processing.

Results

Following the processing of the collected data, a comparison of performance associated with the use of each antenna type was performed. Different aspects of the processing results were analyzed for discrepancies representative of the use of different antenna types as all other hardware and software used in the experiment were homogenous. One characteristic that can be used to assess a GNSS antenna's performance is inspection of the behavior of both the carrier-phase and pseudorange residuals. As these residuals provide insight into the difference between the recorded observables and the modeled values representative of these observables, one can use the plotted residuals to visualize errors in the parameter estimation and/or systematic error mitigation procedures as well as the random measurement errors. A comparison of the estimated carrier-phase and pseudorange residuals for GPS-only and GPS + Galileo processing at 1-, 1.5-, and 2-metre antenna heights for the three antenna types is shown in Figures 5-16. While the visual magnitude of the carrier-phase residuals for each antenna type is nearly the same, a decrease in the visual magnitude of the pseudorange residuals for the Tallysman VP6000 is evident in all cases. Unfortunately, some of the carrier-phase residuals provided in Figures 5-16 demonstrate

anomalous behavior in the form of systematic tails. While the existence of these tails is being investigated, it should also been noted that similar behavior exists in the neutral atmospheric delay estimates for these files. Therefore, the problem may be related to improper handling of GAPS' neutral atmospheric delay estimation procedure. Also, regarding the abnormal behavior of the carrier-phase residuals for the AOA choke-ring antenna in Figures 9 and 15, it is believed that they may be the result of a bird occupying the antenna for a period of time. To eleviate this issue in the future, the use of an appropriate radome is recommended.

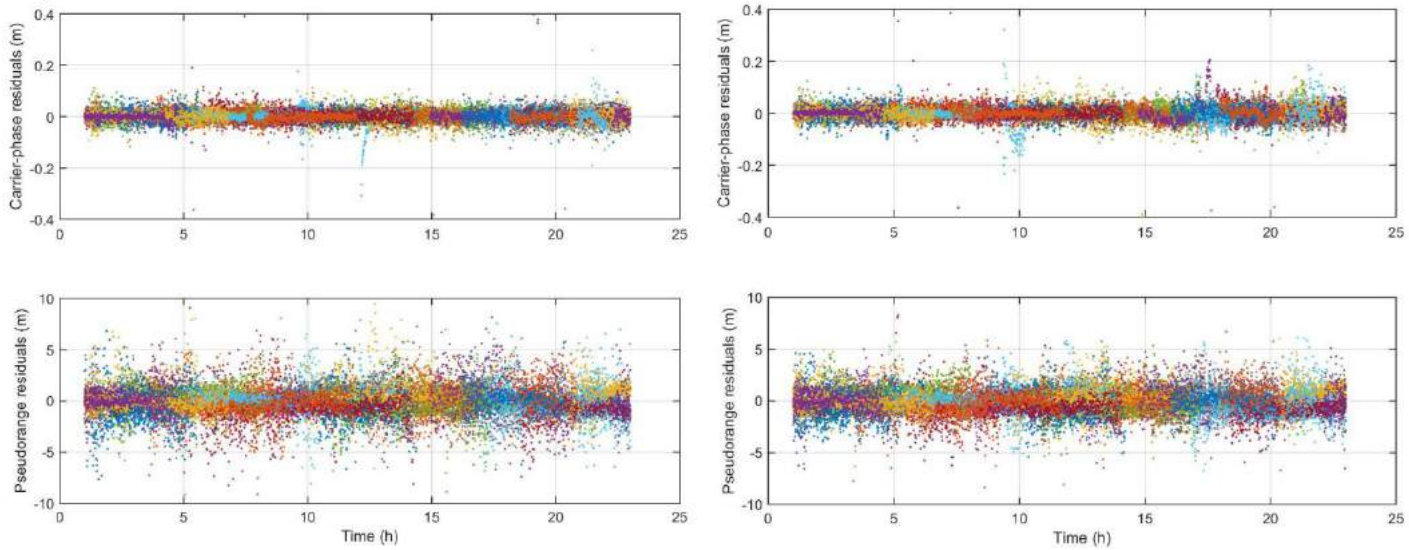

Figure 5: The estimated carrier-phase and pseudorange residuals vs UTC time (GPS-only 1-metre height) for the AOA choke-ring antenna (left) on DOY 278 and the Tallysman VP6000 antenna (right) on DOY 280 of static data collection sessions.

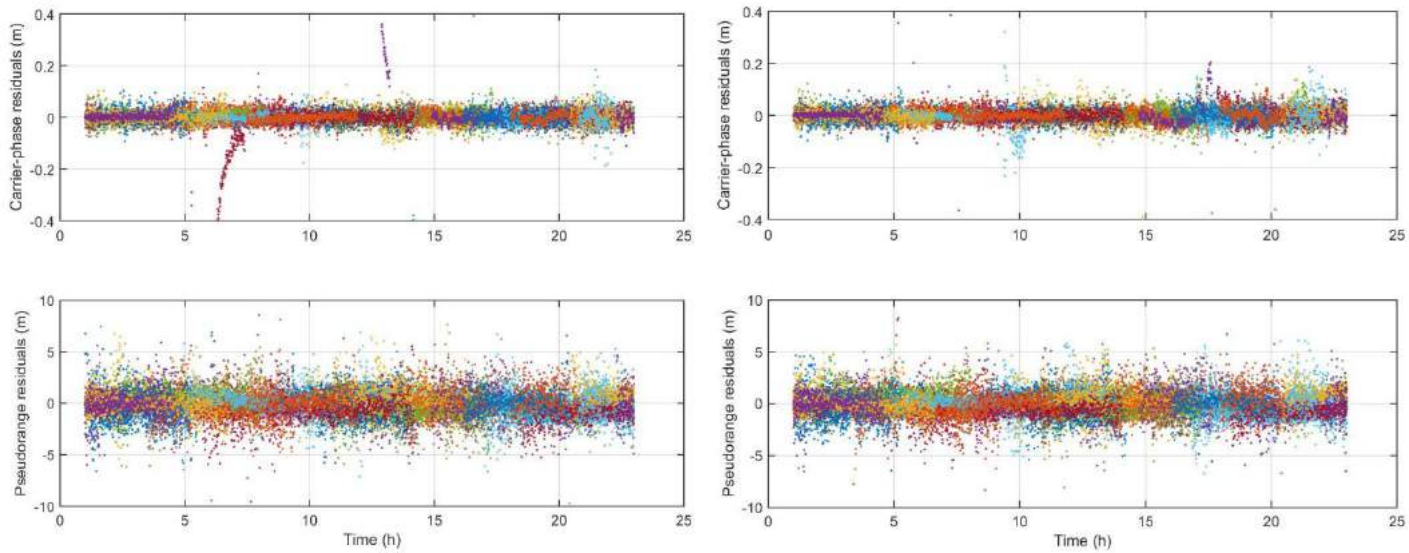

Figure 6: The estimated carrier-phase and pseudorange residuals vs UTC time (GPS-only 1-metre height) for the Leica AX1203+ antenna (left) on DOY 279 and the Tallysman VP6000 antenna (right) on DOY 280 of static data collection sessions.

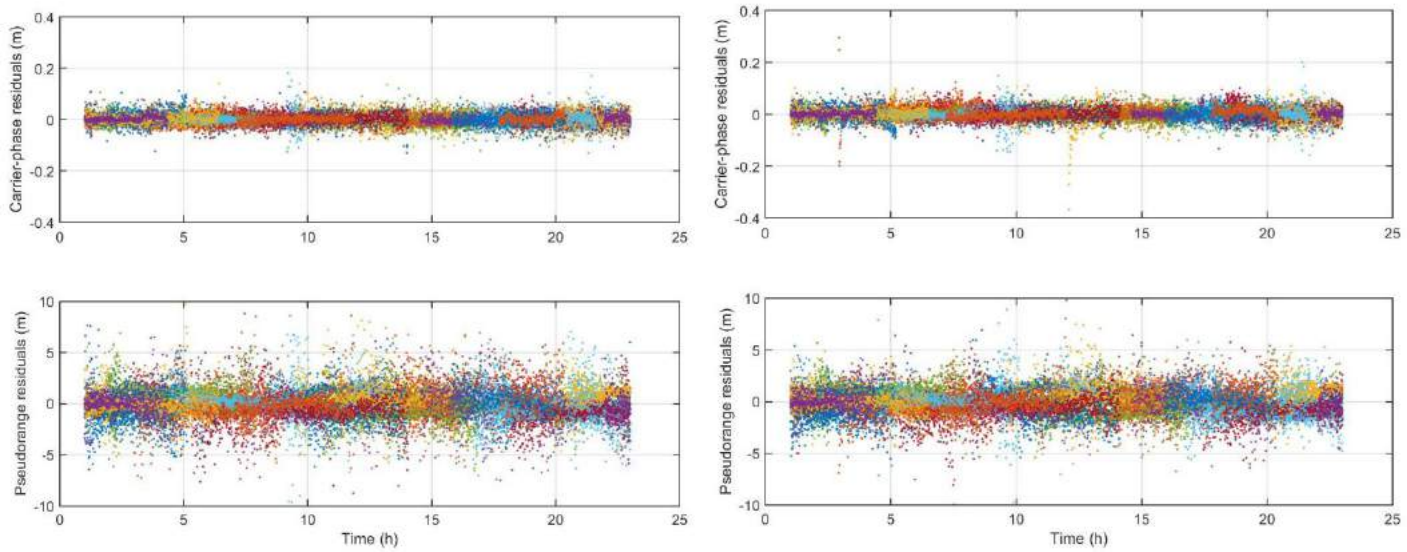

Figure 7: The estimated carrier-phase and pseudorange residuals vs UTC time (GPS-only 2-metre height) for the AOA choke-ring antenna (left) on DOY 284 and the Tallysman VP6000 antenna (right) on DOY 283 of static data collection sessions.

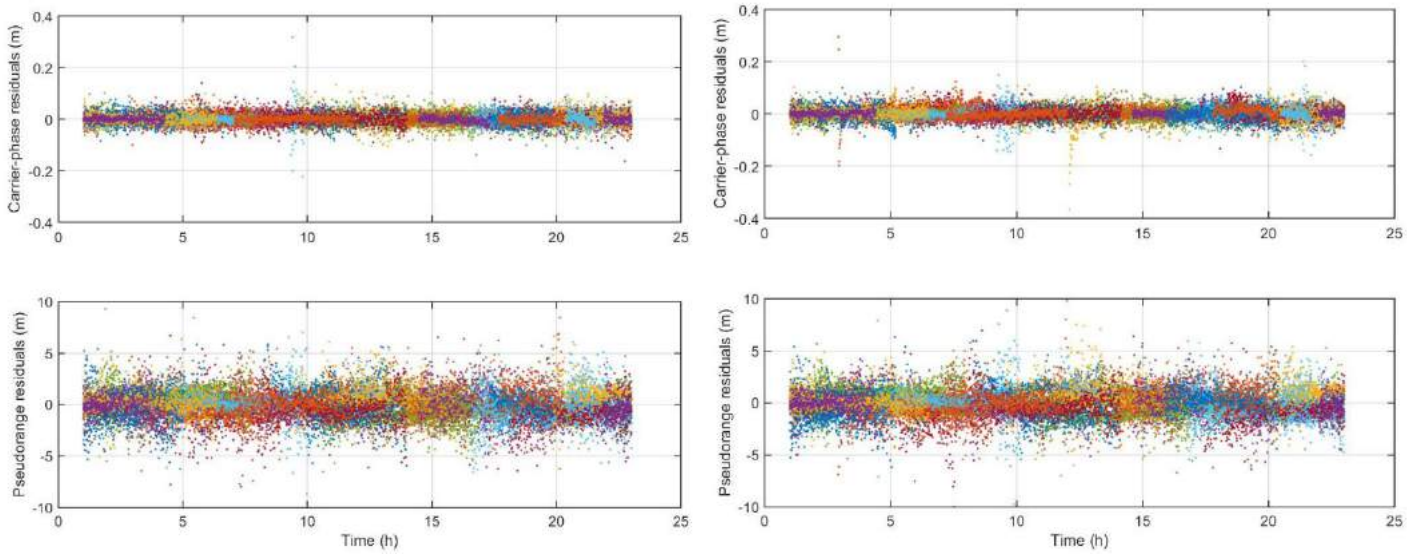

Figure 8: The estimated carrier-phase and pseudorange residuals vs UTC time (GPS-only 2-metre height) for the Leica AX1203+ antenna (left) on DOY 285 and the Tallysman VP6000 antenna (right) on DOY 283 of static data collection sessions.

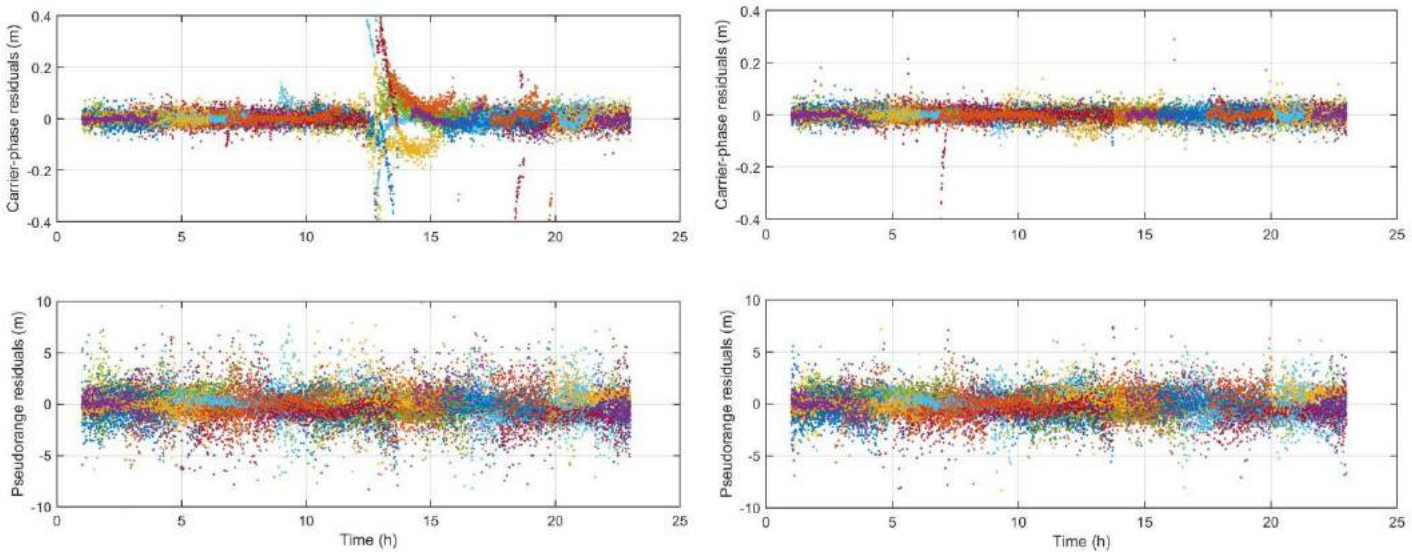

Figure 9: The estimated carrier-phase and pseudorange residuals vs UTC time (GPS-only 1.5-metre height) for the AOA choke-ring antenna (left) on DOY 289 and the Tallysman VP6000 antenna (right) on DOY 288 of static data collection sessions.

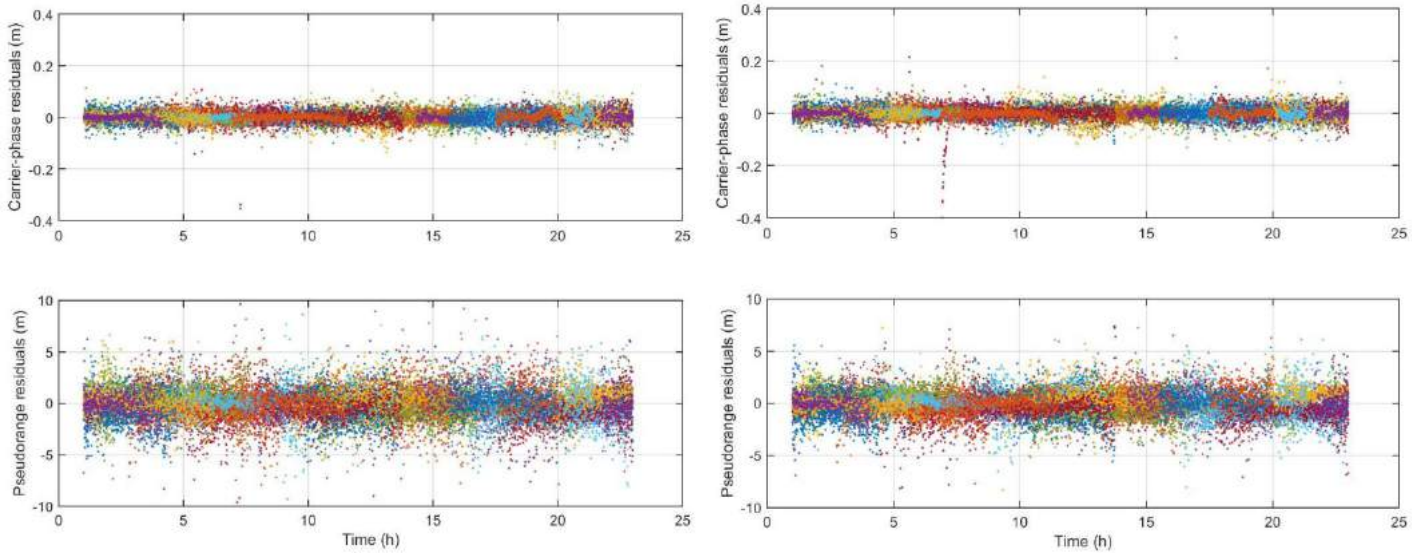

Figure 10: The estimated carrier-phase and pseudorange residuals vs UTC time (GPS-only 1.5-metre height) for the Leica AX1203+ antenna (left) on DOY 287 and the Tallysman VP6000 antenna (right) on DOY 288 of static data collection sessions.

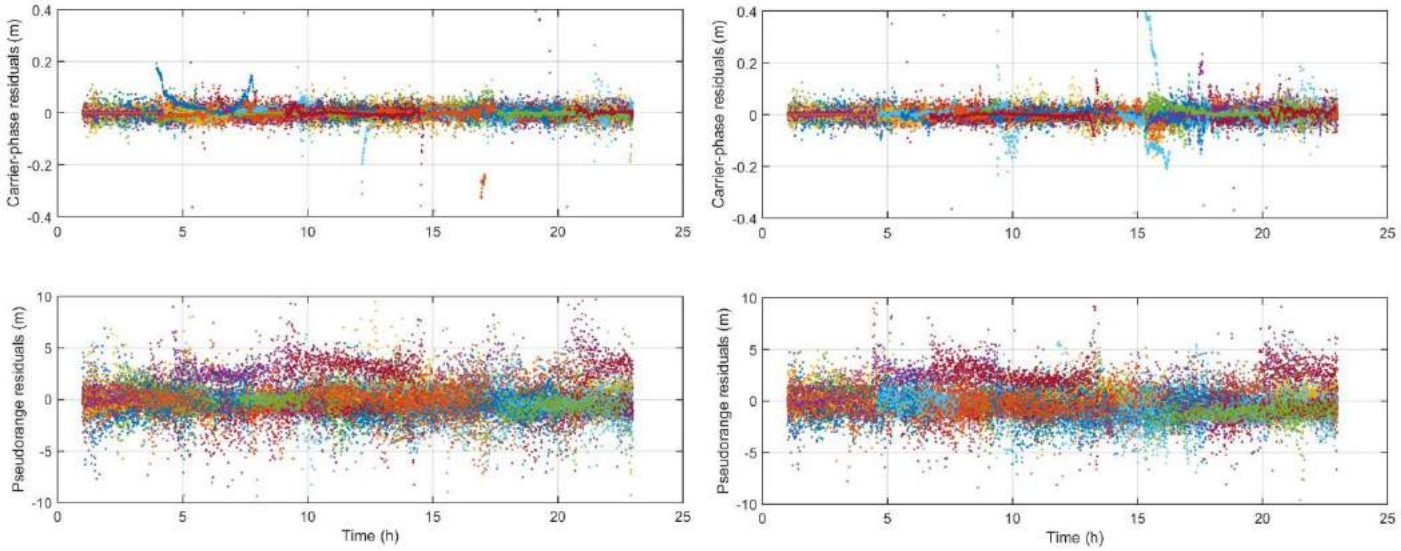

Figure 11: The estimated carrier-phase and pseudorange residuals vs UTC time (GPS + Galileo 1-metre height) for the AOA choke-ring antenna (left) on DOY 278 and the Tallysman VP6000 antenna (right) on DOY 280 of static data collection sessions.

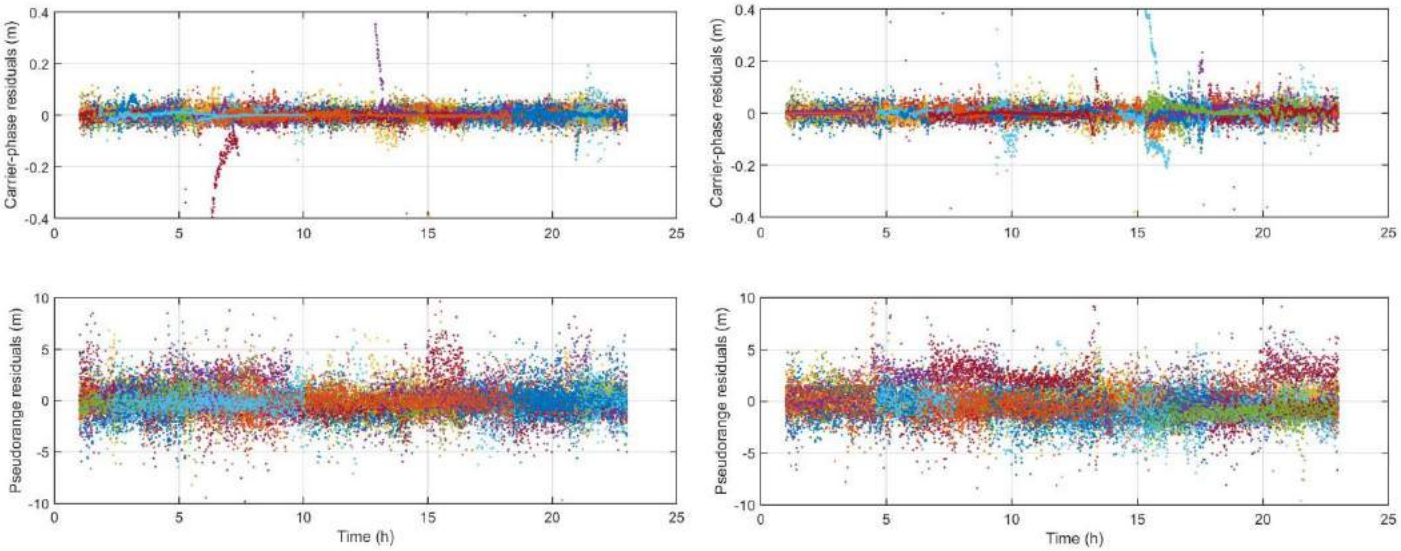

Figure 12: The estimated carrier-phase and pseudorange residuals vs UTC time (GPS + Galileo 1-metre height) for the Leica AX1203+ antenna (left) on DOY 279 and the Tallysman VP6000 antenna (right) on DOY 280 of static data collection sessions.

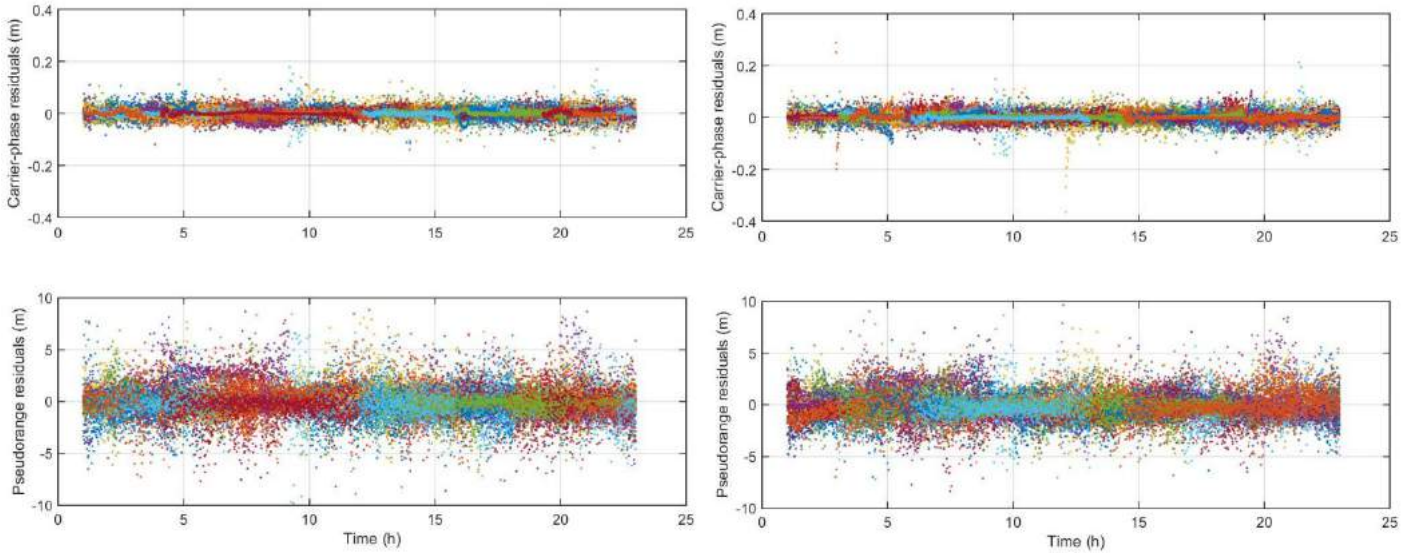

Figure 13: The estimated carrier-phase and pseudorange residuals vs UTC time (GPS + Galileo 2-metre height) for the AOA choke-ring antenna (left) on DOY 284 and the Tallysman VP6000 antenna (right) on DOY 283 of static data collection sessions.

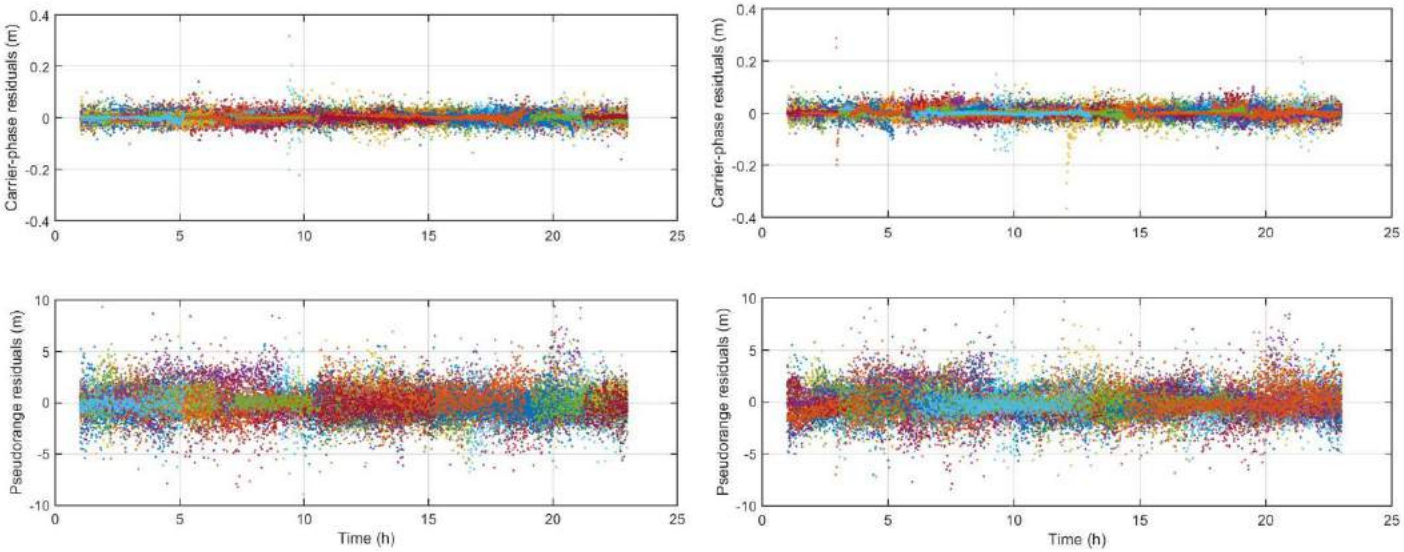

Figure 14: The estimated carrier-phase and pseudorange residuals vs UTC time (GPS + Galileo 2-metre height) for the Leica AX1203+ antenna (left) on DOY 285 and the Tallysman VP6000 antenna (right) on DOY 283 of static data collection sessions.

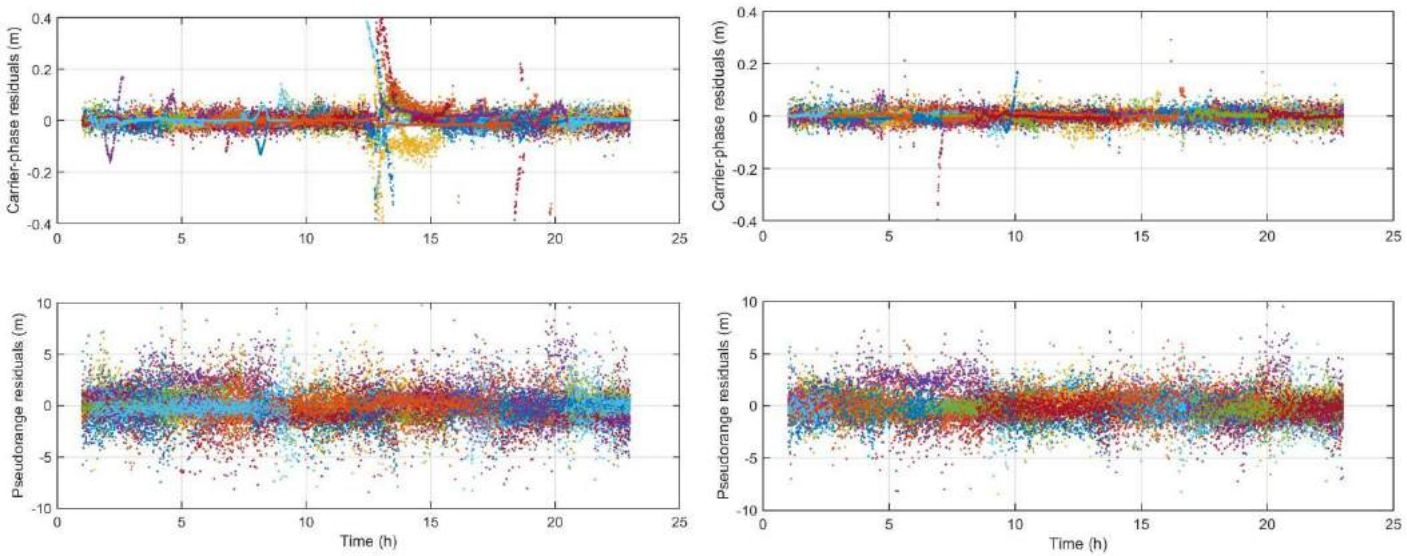

Figure 15: The estimated carrier-phase and pseudorange residuals vs UTC time (GPS + Galileo 1.5-metre height) for the AOA choke-ring antenna (left) on DOY 289 and the Tallysman VP6000 antenna (right) on DOY 288 of static data collection sessions.

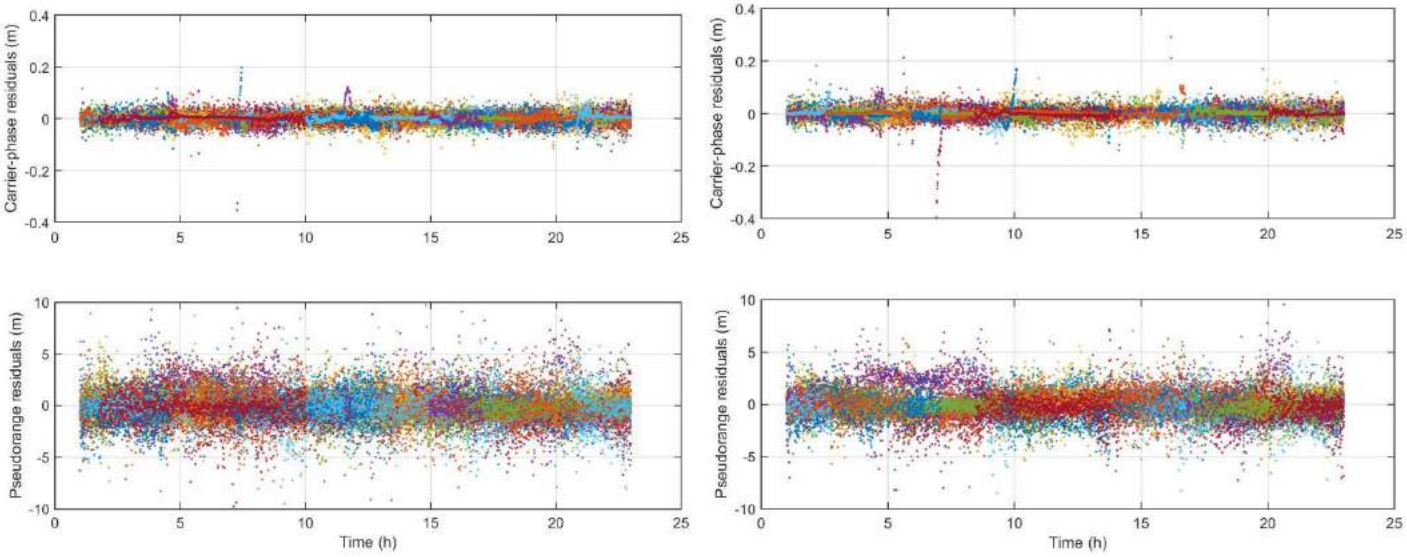

Figure 16: The estimated carrier-phase and pseudorange residuals vs UTC time (GPS + Galileo 1.5-metre height) for the Leica AX1203+ antenna (left) on DOY 287 and the Tallysman VP6000 antenna (right) on DOY 288 of static data collection sessions.

The scatter of the residuals can be quantified by their root-mean-square (RMS) values. Tables 1 and 2 summarize the RMS values of the GPS-only and GPS + Galileo carrier-phase and pseudorange residual estimates at 1-, 1.5-, and 2-metre antenna heights for the Leica AX1203+, AOA choke-ring, and Tallysman VP6000 antennas. For both GPS-only and GPS + Galileo processing, a decrease in magnitude of the RMS of the pseudorange residuals is observed when using the Tallysman VP6000, while the RMS of the carrier-phase residuals is nearly equal in all cases. Such a decrease in the magnitude of the pseudorange residuals may be attributed to the improved multipath mitigation characteristics of the Tallysman VP6000 antenna. There may also be an improved mitigation of carrier-phase multipath with the VP6000, however, it is difficult to assess in the carrier-phase observables, which also reflect other error sources.

Table 1: RMS scatter (metres) of GPS-only carrier-phase and pseudorange residual estimates for the Leica AX1203+, AOA choke-ring, and Tallysman VP6000 antennas at 1-, 1.5-, and 2-metre antenna heights (on three different pillars).

	Leica		AOA		Tallysman	
	Carrier-Phase	Pseudorange	Carrier-Phase	Pseudorange	Carrier-Phase	Pseudorange
1m	0.025	1.466	0.025	1.475	0.036	1.264
	0.031	1.347	0.026	1.495	0.027	1.225
	0.027	1.360	0.028	1.484	0.027	1.263
1.5m	0.022	1.550	0.025	1.480	0.021	1.270
	0.022	1.339	0.021	1.501	0.024	1.252
	0.022	1.388	0.065	1.507	0.027	1.256
2m	0.024	1.555	0.023	1.483	0.027	1.319
	0.024	1.337	0.021	1.527	0.021	1.250
	0.021	1.401	0.020	1.476	0.026	1.241
Avg.	0.024	1.416	0.028	1.492	0.026	1.260

Table 2: RMS scatter (metres) of GPS + Galileo carrier-phase and pseudorange residual estimates for the Leica AX1203+, AOA choke-ring, and Tallysman VP6000 antennas at 1-, 1.5-, and 2-metre antenna heights (on three different pillars).

	Leica		AOA		Tallysman	
	Carrier-Phase	Pseudorange	Carrier-Phase	Pseudorange	Carrier-Phase	Pseudorange
1m	0.024	1.496	0.025	1.644	0.037	1.464
	0.030	1.436	0.025	1.538	0.023	1.336
	0.025	1.519	0.027	1.690	0.031	1.547
1.5m	0.020	1.526	0.022	1.507	0.019	1.295
	0.020	1.397	0.019	1.536	0.024	1.306
	0.021	1.406	0.055	1.532	0.029	1.342
2m	0.021	1.556	0.021	1.507	0.023	1.359
	0.022	1.332	0.018	1.489	0.019	1.284
	0.018	1.418	0.019	1.501	0.023	1.300
Avg.	0.022	1.454	0.026	1.549	0.025	1.359

Being that each antenna was intentionally subjected to significant multipath interference via several adjacent multipath surfaces, observables from each observation session and antenna type were used to estimate the magnitude of L1 and L2 pseudorange multipath. This was done using an existing code multipath estimation utility within GAPS (Leandro, 2009). Figures 17-22 show overall multipath noise versus satellite elevation angle for the GPS L1 and L2 pseudorange observables for the Leica AX1203+, AOA choke-ring, and Tallysman VP6000 antennas at 1-, 1.5-, and 2-metre antenna heights where multipath noise estimates have been binned by elevation angle as (10,20] plotted as 15°, (20,30] as 25° and so on. In each case, a significant decrease in estimated multipath noise is evident when using the Tallysman VP6000, particularly at lower receiver-satellite elevation angles (<30°).

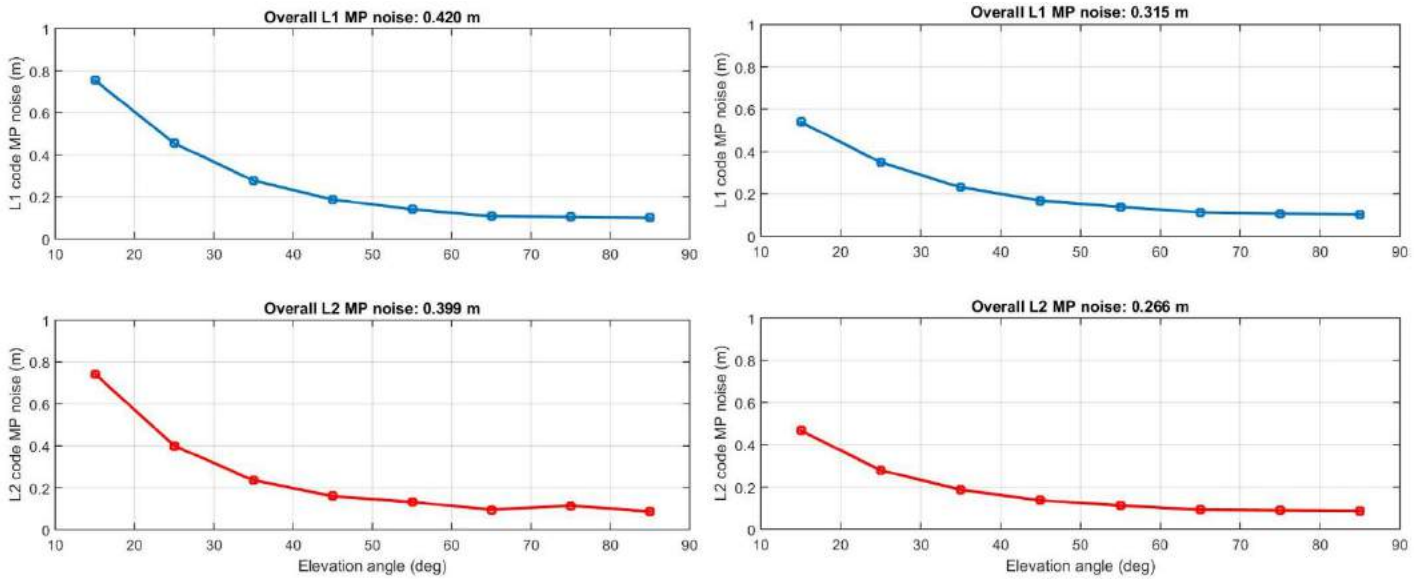

Figure 17: Estimated GPS L1 and L2 code multipath vs elevation angle for all used satellites (1-metre antenna height) for both the AOA choke-ring antenna (left) and the Tallysman VP6000 antenna (right) static data collection sessions on DOY 279 and 278, respectively.

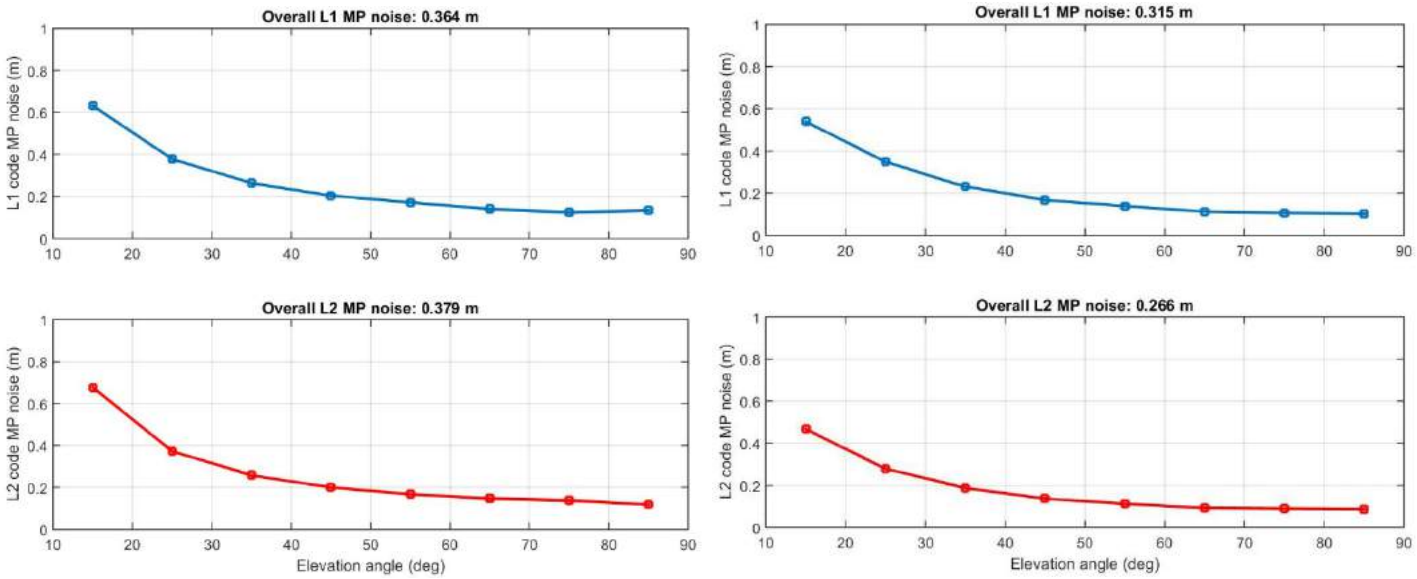

Figure 18: Estimated GPS L1 and L2 code multipath vs elevation angle for all used satellites (1-metre antenna height) for both the Leica AX1203+ antenna (left) and the Tallysman VP6000 antenna (right) static data collection sessions on DOY 280 and 278, respectively.

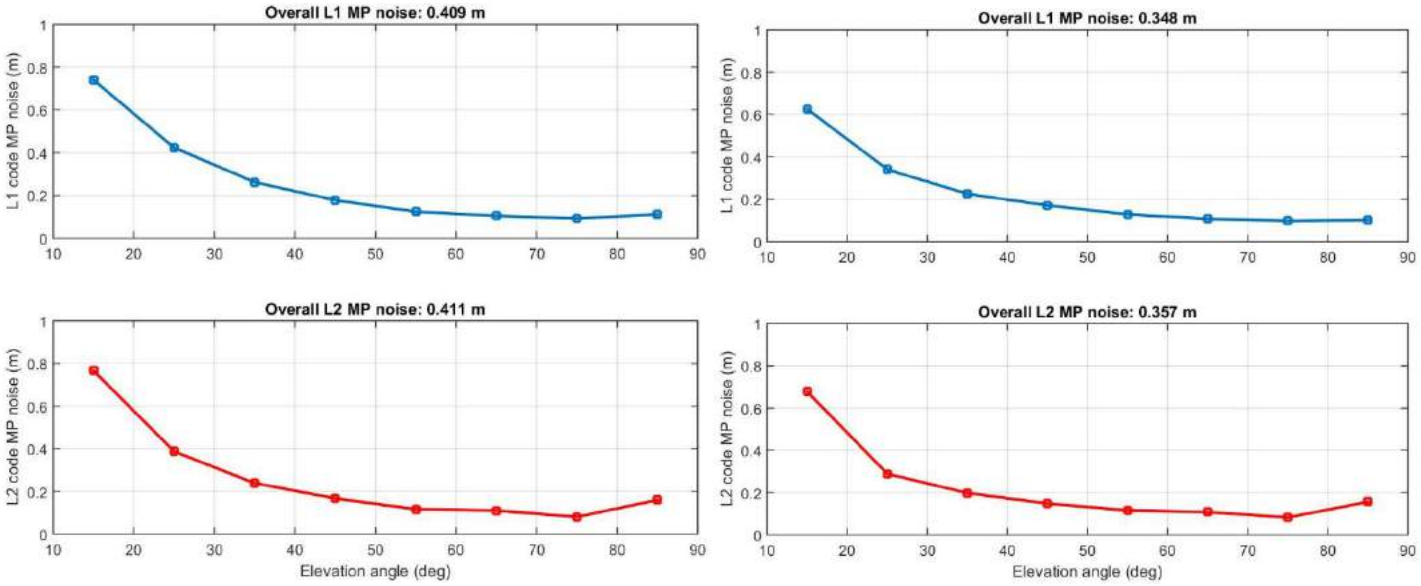

Figure 19: Estimated GPS L1 and L2 code multipath vs elevation angle for all used satellites (1.5-metre antenna height) for both the AOA choke-ring antenna (left) and the Tallysman VP6000 antenna (right) static data collection sessions on DOY 285 and 284, respectively.

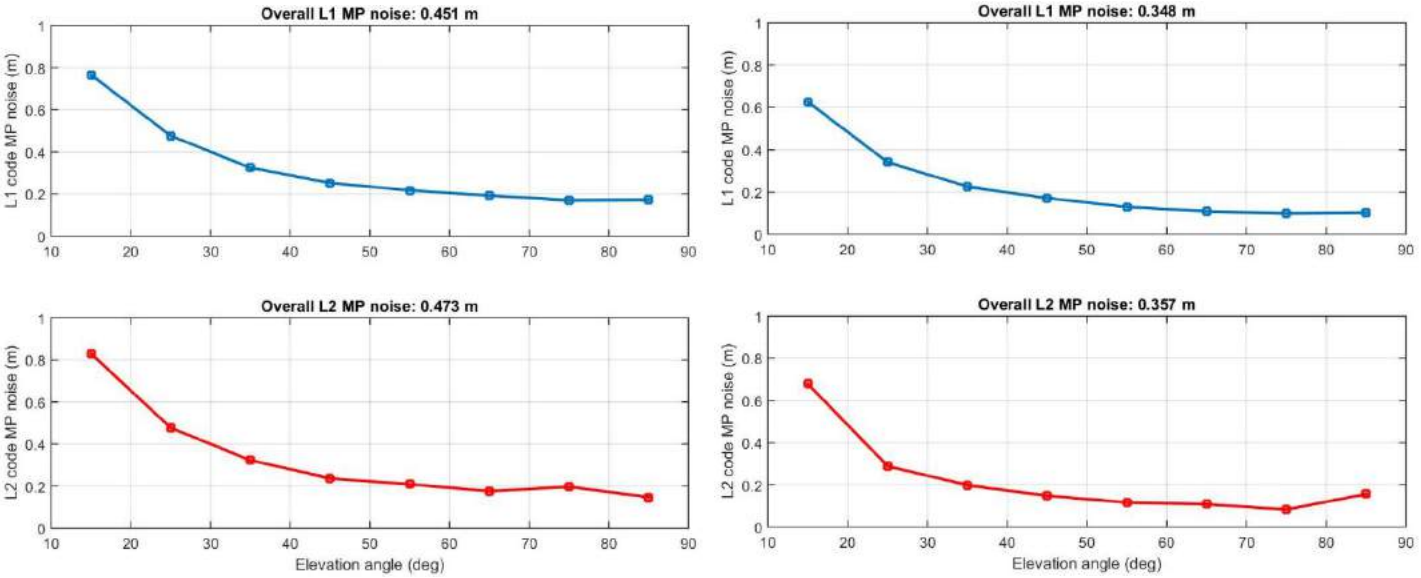

Figure 20: Estimated GPS L1 and L2 code multipath vs elevation angle for all used satellites (1.5-metre antenna height) for both the Leica AX1203+ antenna (left) and the Tallysman VP6000 antenna (right) static data collection sessions on DOY 283 and 284, respectively.

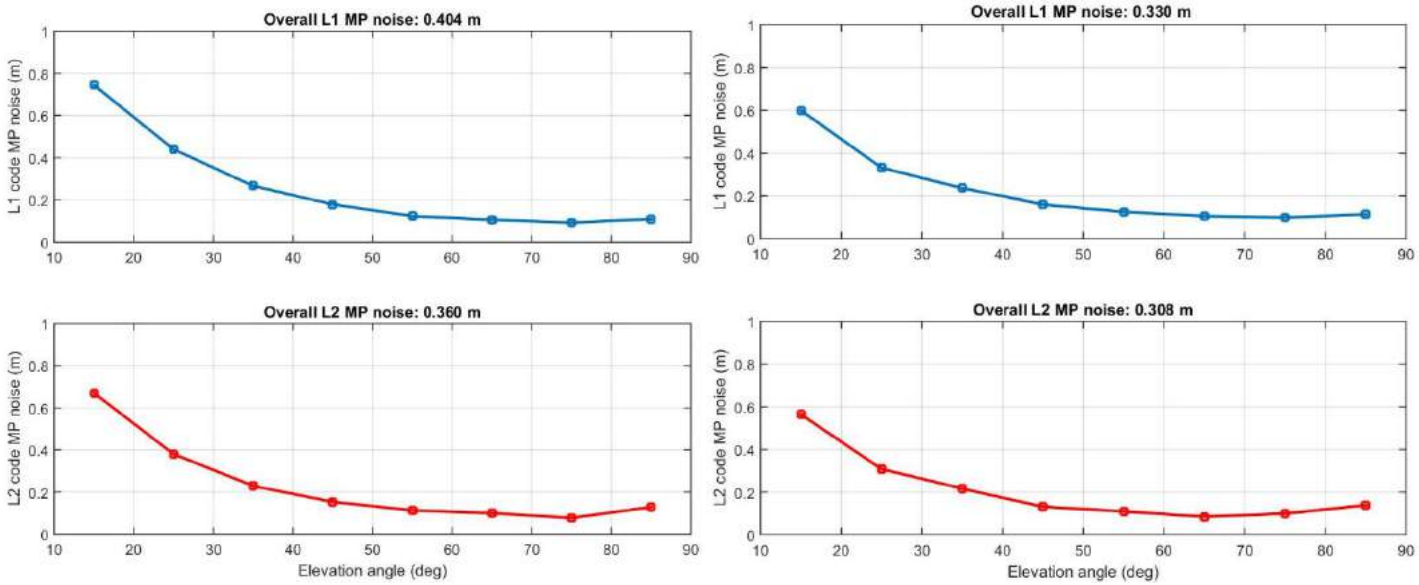

Figure 21: Estimated GPS L1 and L2 code multipath vs elevation angle for all used satellites (2-metre antenna height) for both the AOA choke-ring antenna (left) and the Tallysman VP6000 antenna (right) static data collection sessions on DOY 287 and 289, respectively.

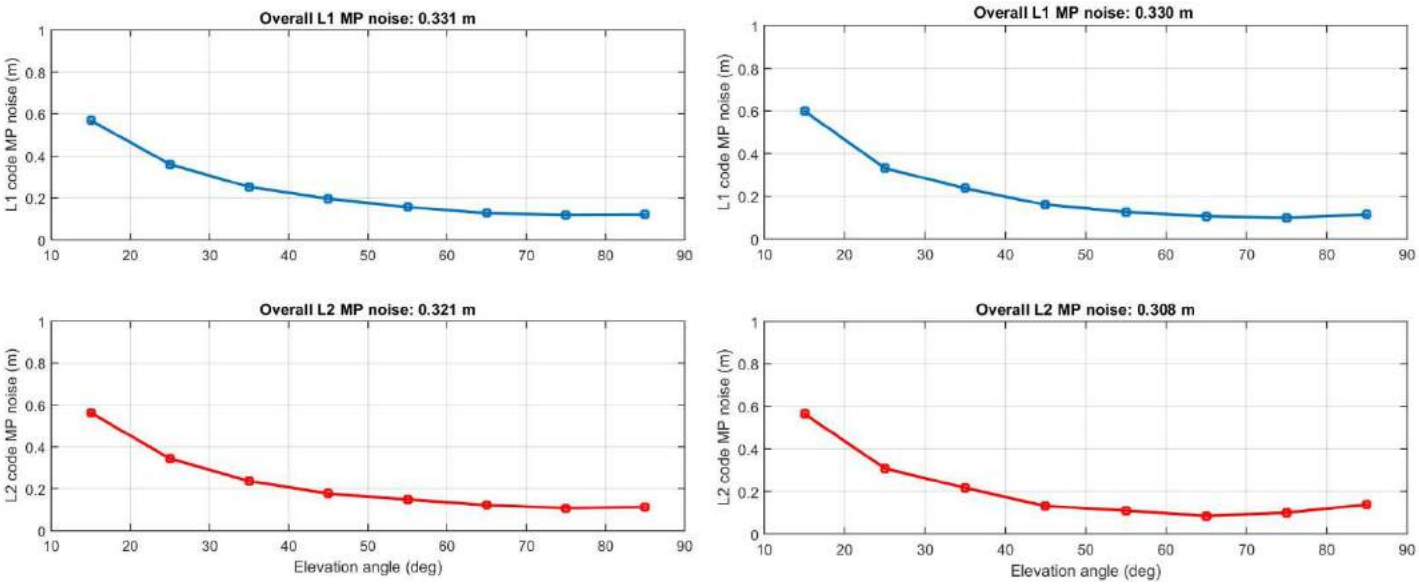

Figure 22: Estimated GPS L1 and L2 code multipath vs elevation angle for all used satellites (2-metre antenna height) for both the Leica AX1203+ antenna (left) and the Tallysman VP6000 antenna (right) static data collection sessions on DOY 288 and 289, respectively.

Figures 23-28 show multipath noise and elevation angle versus time for GPS PRN 6, PRN 19, and PRN 28 L1 and L2 pseudorange observables, respectively, for the Leica AX1203+, AOA choke-ring, and Tallysman VP6000 antennas at 1-, 1.5-, and 2-metre antenna heights. Again, a significant decrease in estimated multipath noise, as evidenced by 1-sigma standard deviation values, are evident when using the Tallysman VP6000, particularly at lower receiver-satellite elevation angles (<30°).

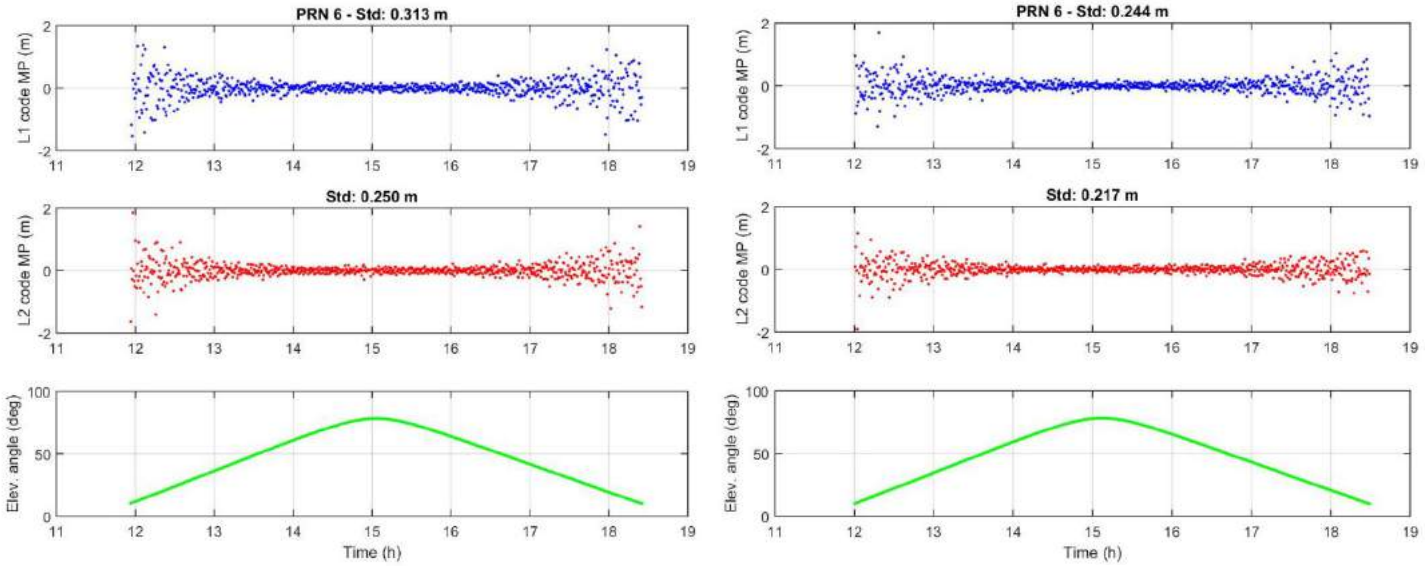

Figure 23: The estimated GPS PRN 6 L1 and L2 code multipath and elevation angle vs UTC time (1-metre antenna height) for both the AOA choke-ring antenna (left) and the Tallysman VP6000 antenna (right) static data collection sessions on DOY 279 and 278, respectively.

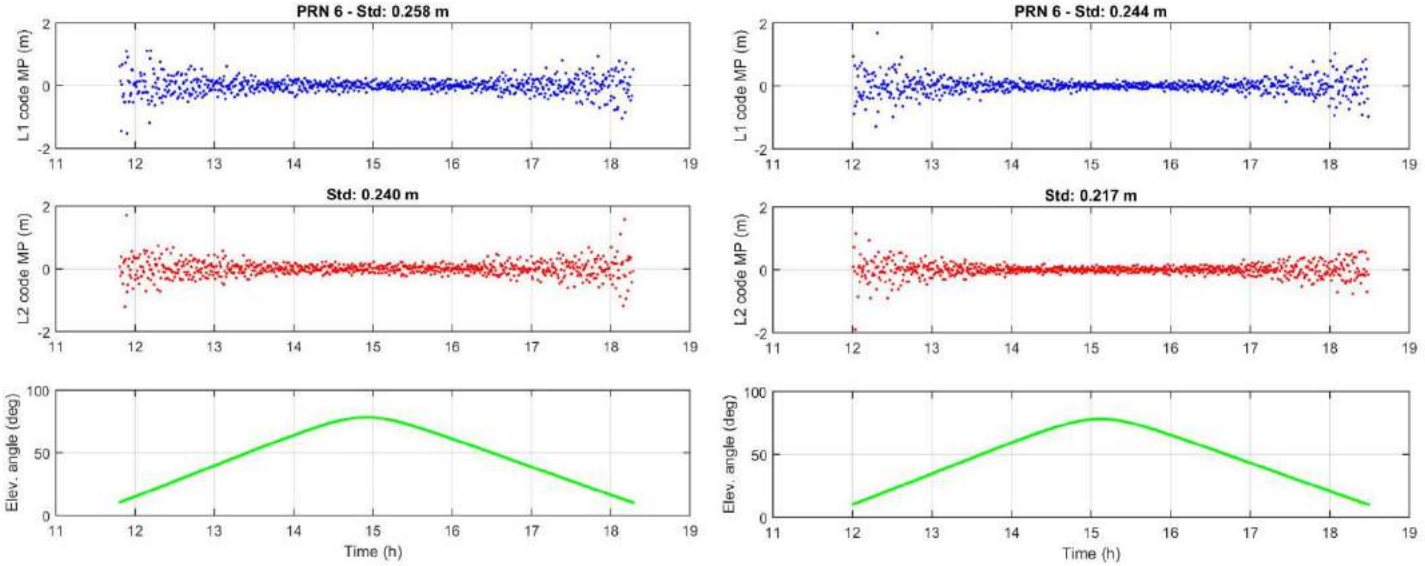

Figure 24: The estimated GPS PRN 6 L1 and L2 code multipath and elevation angle vs UTC time (1-metre antenna height) for both the Leica AX1203+ antenna (left) and the Tallysman VP6000 antenna (right) static data collection sessions on DOY 280 and 278, respectively.

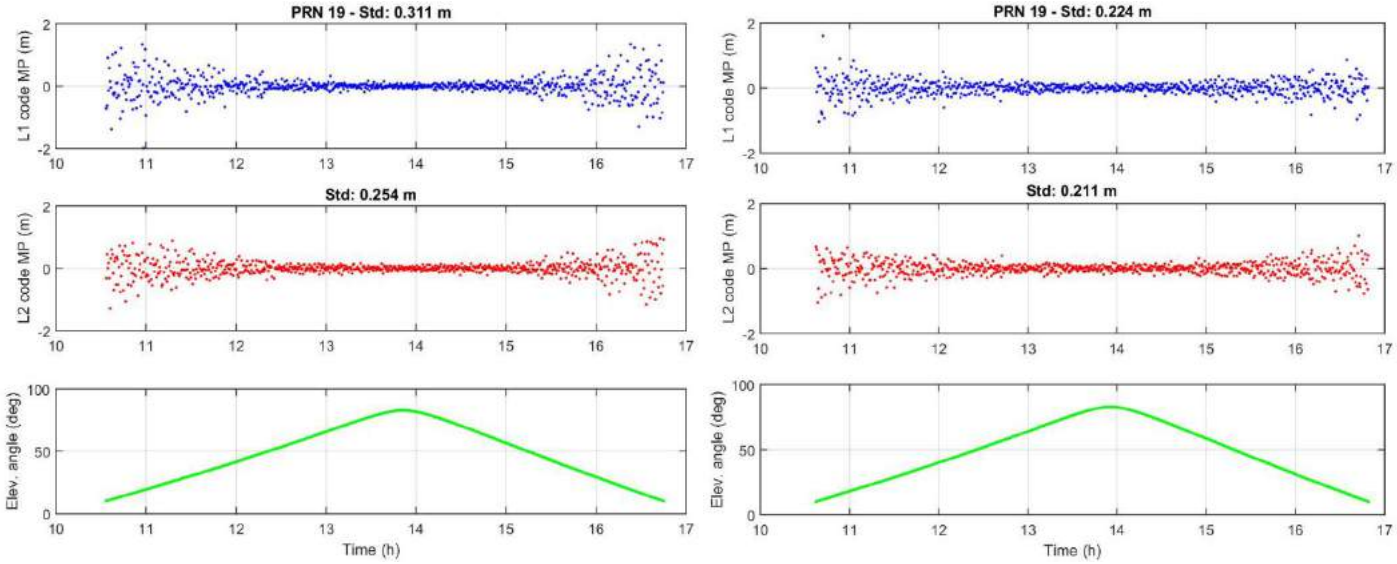

Figure 25: The estimated GPS PRN 19 L1 and L2 code multipath and elevation angle vs UTC time (1.5-metre antenna height) for both the AOA choke-ring antenna (left) and the Tallysman VP6000 antenna (right) static data collection sessions on DOY 285 and 284, respectively.

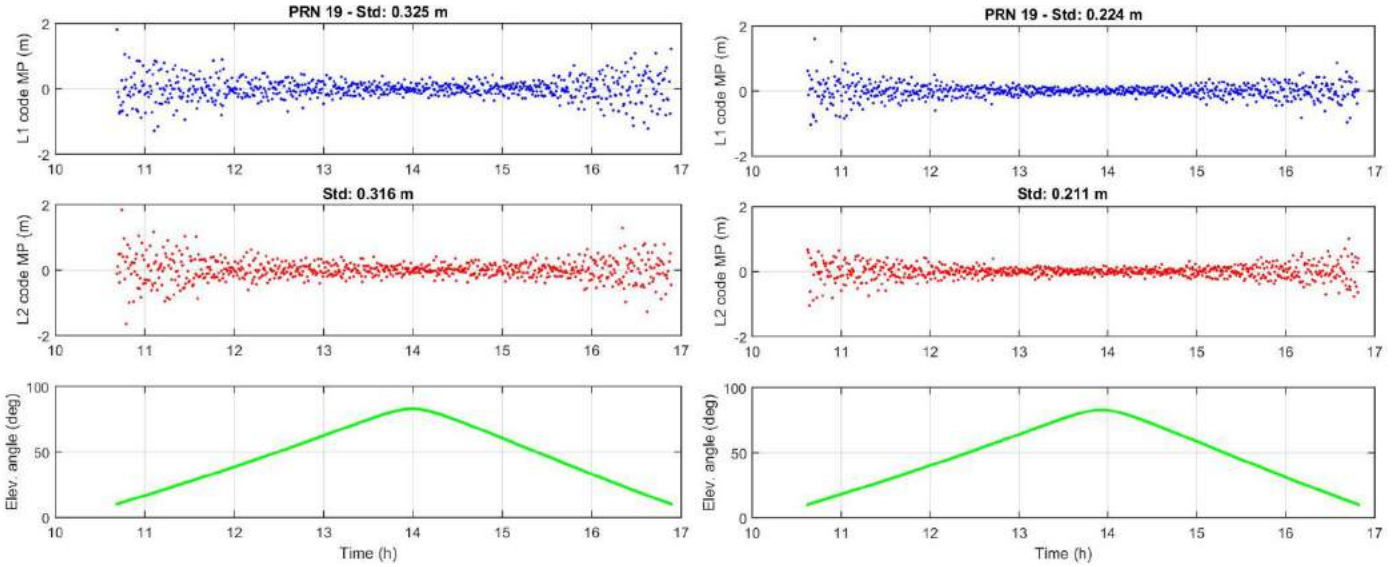

Figure 26: The estimated GPS PRN 19 L1 and L2 code multipath and elevation angle vs UTC time (1.5-metre antenna height) for both the Leica AX1203+ antenna (left) and the Tallysman VP6000 antenna (right) static data collection sessions on DOY 283 and 284, respectively.

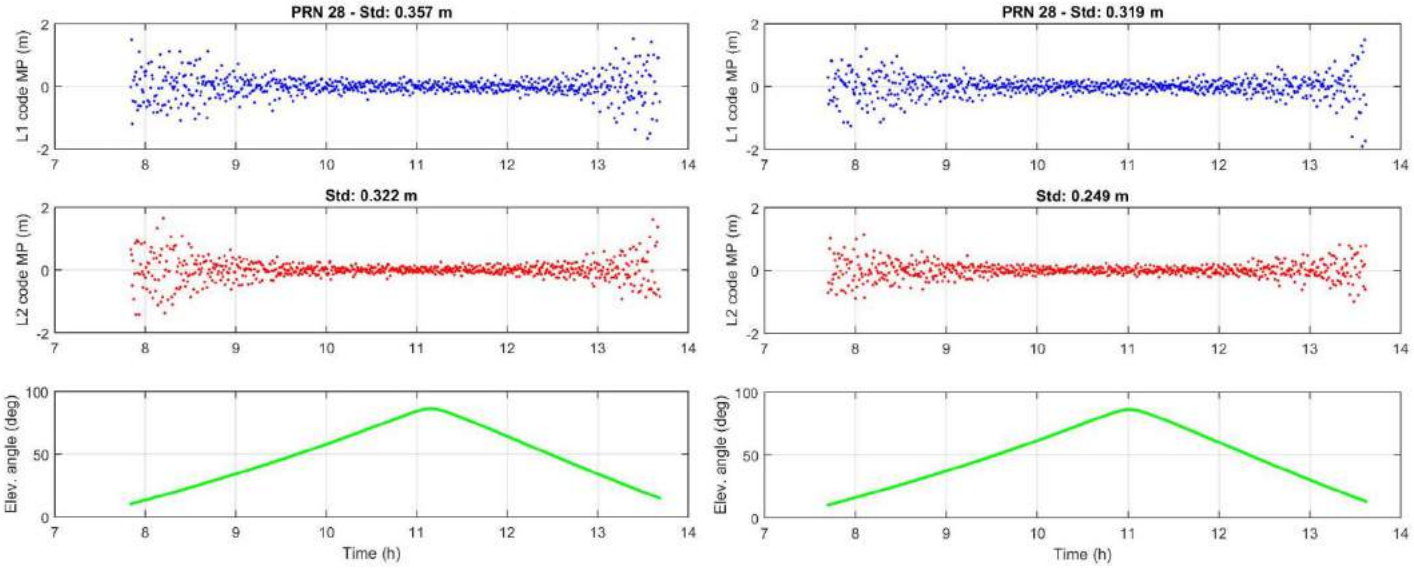

Figure 27: The estimated GPS PRN 28 L1 and L2 code multipath and elevation angle vs UTC time (2-metre antenna height) for both the AOA choke-ring antenna (left) and the Tallysman VP6000 antenna (right) static data collection sessions on DOY 287 and 289, respectively.

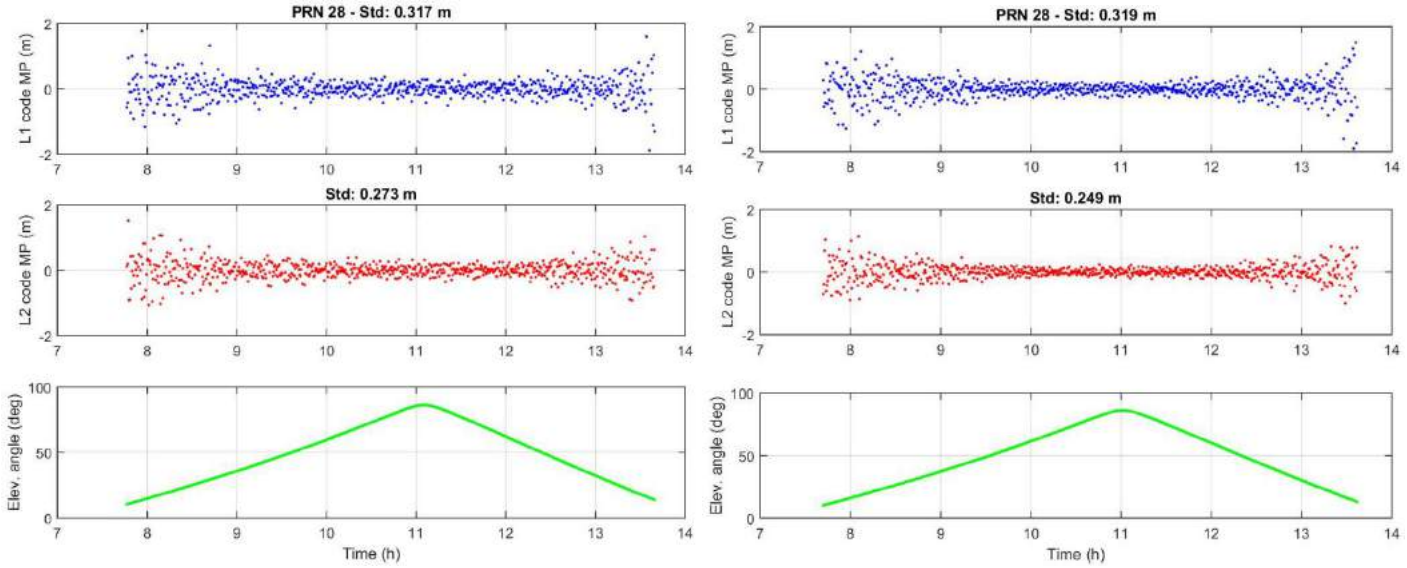

Figure 28: The estimated GPS PRN 28 L1 and L2 code multipath and elevation angle vs UTC time (2-metre antenna height) for both the Leica AX1203+ antenna (left) and the Tallysman VP6000 antenna (right) static data collection sessions on DOY 288 and 289, respectively.

Conclusions

Following the processing of the GNSS data from our static experiment collected in a known high-multipath environment using a Leica AX1203+, a Tallysman VP6000, and a AOA choke-ring antenna, analysis of several metrics provided insight into the difference in performance associated with the use of each antenna type. When comparing GAPS' processing results for each antenna type, it is clear that use of the VP6000 antenna provided a significant decrease in multipath noise for both the GPS L1 and L2 and Galileo L1 and L5 pseudorange observables. The VP6000 antenna also provided lower RMS values for the pseudorange residuals than the AOA choke-ring antenna with nearly equal carrier-phase residual estimates.

References

Blewitt, G. (1990). An automatic editing algorithm for GPS data. *Geophysical Research Letters*. 17(3):199–202, DOI: 10.1029/GL017i003p00199.

Boehm, J., Werl, B., and Schuh, H. (2006). Troposphere Mapping Functions for GPS and Very Long Baseline Interferometry From European Centre for Medium-Range Weather Forecasts Operational Analysis Data. *Journal of Geophysical Research*, 111, B02406, DOI:10.1029/2005JB003629.

Leandro, R. F. (2009). *Precise Point Positioning with GPS: A New Approach for Positioning, Atmospheric Studies, and Signal Analysis.* Ph.D. dissertation, Department of Geodesy and Geomatics Engineering, Technical Report No. 267, University of New Brunswick, Fredericton, New Brunswick, Canada, 232 pp.

Montenbruck, O., Steigenberger, P., Khachikyan, R., Weber, G., Langley, R.B., Mervart, L., Hugentobler, U. (2014). IGS-MGEX: Preparing the Ground for Multi-Constellation GNSS Science. *Inside GNSS.* 9(1):42-49.

Nievinski, Felipe G. (2009). *Ray-tracing Options to Mitigate the Neutral Atmosphere Delay in GPS*. M.Sc.E. thesis, Department of Geodesy and Geomatics Engineering Technical Report No. 262, University of New Brunswick, Fredericton, New Brunswick, Canada, 213 pp.

Schmid, R., Mader, G., Herring, T. (2005). From relative to absolute antenna phase center corrections. In: Meindl, M. (ed.) Proceedings of the IGS Workshop and Symposium 2004, Bern.

White, R.M., Langley, R.B. (2015). Precise Point Positioning with Galileo Observables. 5th International Colloquium, Scientific and Fundamental Aspects of the Galileo Programme, Braunschweig, Germany, 27-29 October.

White, R.M., Langley, R.B. (2017a). Kinematic Testing and Analysis of the Tallysman VeraPhase VP6000 GNSS Antenna. University of New Brunswick, Fredericton, New Brunswick, Canada.

White, R.M., Langley, R.B. (2017b). Preliminary Static Testing and Analysis of the Tallysman VeraPhase VP6000 GNSS Antenna. University of New Brunswick, Fredericton, New Brunswick, Canada.